VIII: Dust

A. Motivations

- Dust plays a vital role in nearly all aspects of astrophysics
- This includes simple observations (reddening, extinction)
- And basic physical processes, e.g. heating and cooling
- A full course could be devoted to the topic. We will discuss only the basics here.

B. ISM Abundances: Oxygen

- Why should we study ISM metals to learn about dust?
  - ◇ Dust is composed of metals, i.e. no metals = no dust
  - ◇ A discussion of the metals in the ISM will motivate the presence of dust
- Why begin with Oxygen?
  - ◇ It is the most abundant metal (by number)
  - ◇ Solar abundances (aside)
    - ▲ Mainly derived from meteoritic abundances
    - ▲ e.g. Anders & Grevesse
    - ▲ Table (logarithmic scale ϵ_X with H=12)

Al	6.49	13			
Ar	6.52	18			
As	2.37	33			
B	2.79	5			
Ba	2.22	56			
C	8.59	6			
Ca	6.35	20	Na	6.32	11
Ce	1.61	58	Ne	8.08	10
Cd	1.76	48	Nd	1.47	60
Cl	5.28	17	Ni	6.25	28
Co	4.91	27	O	8.74	8
Cr	5.67	24	P	5.53	15
Cu	4.29	29	Pb	2.06	82
Eu	0.54	63	Rb	2.41	37
Fe	7.50	26	S	7.20	16
Ga	3.13	31	Sc	3.10	21
Ge	3.63	32	Si	7.56	14
H	12.00	1	Sm	0.97	62
K	5.13	19	Sn	2.14	50
Kr	3.23	36	Te	2.24	52
La	1.22	57	Ti	4.94	22
Li	3.31	3	Tl	0.83	81
Mg	7.58	12	V	4.02	23
Mn	5.53	25	Xe	2.23	54
Mo	1.97	42	Y	2.23	39
N	7.93	7	Zn	4.67	30

- Observing Oxygen in the ISM

- ◇ Study O^0
  - ▲ O^0 is the dominant ionization state of O in a neutral gas
  - ▲ Furthermore, charge-exchange reactions imply $O^0/H^0 = O/H$
- ◇ Focus on the OIλ1355 transition
  - ▲ Semi-forbidden line with $f_{1355} = 1.25 \times 10^{-6}$
  - ▲ Why such an 'unusual' transition?
    - ○ Consider OIλ1302 with $f_{1302} = 0.049$
    - ○ Approximate column density

$$\log N_O = \log N_H - 12 + \epsilon_O \quad (1)$$
$$\approx 21 - 12 + 8.74 \quad (2)$$
$$= 17.7 \quad (3)$$

    - ○ Central optical depth of OI 1302

$$\tau_0^{1302} = \frac{1.497 \times 10^{-2}}{b} N_j \lambda f_{jk} \quad (4)$$
$$\approx 9500 (b/5\,\mathrm{km/s})^{-1} \quad (5)$$

    - ○ For the same gas cloud, OI λ1355 has

$$\tau_0^{1355} \approx 0.2 \quad (6)$$

  - ▲ This implies that the OI 1355 transition lies on the weak portion of the COG ($N \propto W_\lambda$)

- Meyer et al. (1998, ApJ, 493, 222): HST/GHRS observations of Oxygen
  - ◇ High resolution
  - ◇ High SNR
  - ◇ Fig

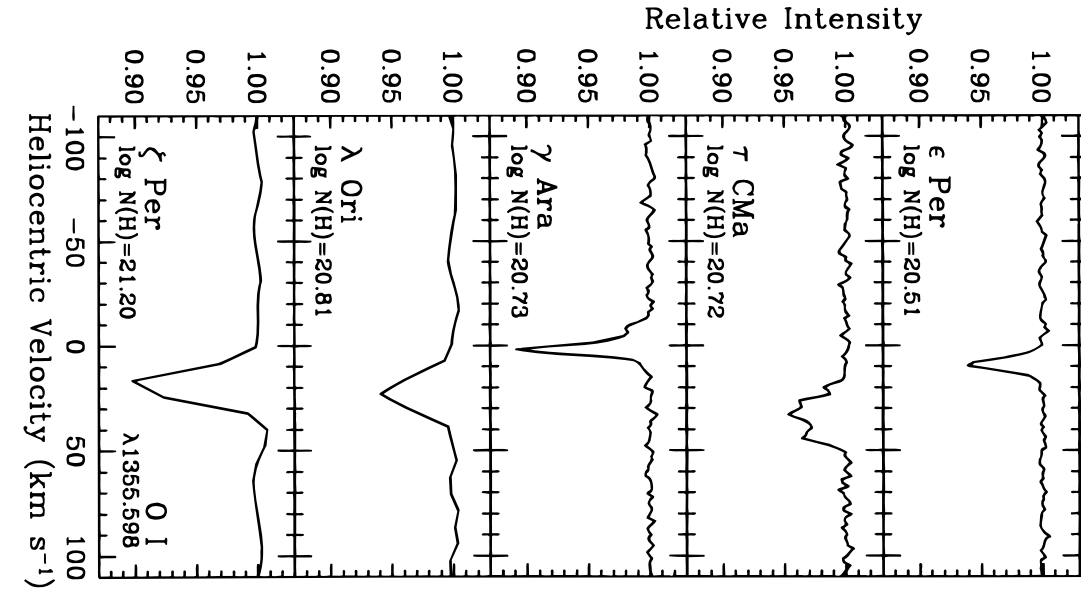

FIG. 1.—*HST* GHRS spectra of the interstellar O I λ1355.598 absorption line toward γ Cas, δ Ori, ϵ Per, τ CMa, and γ Ara at a velocity resolution of 3.5 km s^{-1} and toward λ Ori and ζ Per at a resolution of 16 km s^{-1}. The spectra are displayed from top to bottom in order of increasing total hydrogen column density in the observed sight lines. The mea-

◇ Table

TABLE 1

GHRS Interstellar Oxygen Abundances

Star	N(H)[a] (cm^{-2})	log n_H[b] (cm^{-3})	log $f(H_2)$[c]	W_λ(1356)[d] (mÅ)	N(O I)[e] (cm^{-2})	10^6 O/H[f]
γ Cas	1.5 (0.2) × 10^{20}	−0.60	< −2.36	1.1 (0.1)	5.4 (0.5) × 10^{16}	367 (62)
ζ Per	1.6 (0.2) × 10^{21}	0.11	−0.23	8.0 (0.5)	4.8 (0.6) × 10^{17}	306 (49)
ϵ Per	3.3 (0.5) × 10^{20}	−0.46	−0.69	2.1 (0.2)	1.0 (0.1) × 10^{17}	316 (53)
ξ Per	1.9 (0.2) × 10^{21}	0.18	−0.44	10.8 (1.3)	6.0 (0.8) × 10^{17}	321 (53)
δ Ori	1.6 (0.2) × 10^{20}	−0.87	−5.21	0.9 (0.1)	4.4 (0.5) × 10^{16}	282 (46)
λ Ori	6.5 (1.2) × 10^{20}	−0.38	−1.39	4.0 (0.5)	2.0 (0.3) × 10^{17}	316 (71)
ι Ori	1.5 (0.2) × 10^{20}	−1.02	−5.17	1.1 (0.2)	5.4 (1.0) × 10^{16}	370 (81)
ϵ Ori	2.9 (0.4) × 10^{20}	−0.73	−3.59	1.8 (0.2)	8.9 (1.0) × 10^{16}	307 (55)
κ Ori	3.4 (0.3) × 10^{20}	−0.66	−4.55	2.1 (0.2)	1.0 (0.1) × 10^{17}	303 (40)
15 Mon.....	2.3 (0.4) × 10^{20}	−0.97	−4.52	1.3 (0.3)	6.4 (1.5) × 10^{16}	278 (81)
τ CMa	5.3 (0.4) × 10^{20}	−0.95	−4.95	4.0 (0.3)	2.0 (0.2) × 10^{17}	372 (40)
ζ Oph.....	1.4 (0.1) × 10^{21}	0.52	−0.20	6.4 (0.6)	4.0 (0.4) × 10^{17}	284 (32)
γ Ara	5.4 (0.6) × 10^{20}	−0.59	−1.20	3.9 (0.2)	2.0 (0.2) × 10^{17}	378 (51)

[a] $N(H) = 2N(H_2) + N(H\ I)$ is the total hydrogen column density ($\pm 1\ \sigma$) in the observed sight lines. These values reflect the H_2 column densities measured by Savage et al. 1977 and the weighted means of the Bohlin, Savage, & Drake 1978 and Diplas & Savage 1994 N(H I) data.

[b] Mean hydrogen sight line density is calculated from N(H) and the stellar distances.

[c] $f(H_2) = 2N(H_2)/N(H)$ is the fractional abundance of hydrogen nuclei in H_2 in the observed sight lines.

[d] Measured equivalent widths ($\pm 1\ \sigma$) of the O I 1355.598 Å absorption line.

[e] Derived O I column densities ($\pm 1\ \sigma$) in the observed sight lines. The ξ Per and ζ Oph values are taken from the analyses of Cardelli et al. 1991 and Savage, Cardelli, & Sofia 1992. The ζ Per, λ Ori, and γ Ara values are corrected for a slight amount of saturation using respective Gaussian b-values ($\pm 1\ \sigma$) of $2.0^{+2.0}_{-0.5}$, $5.0^{+\infty}_{-2.5}$, and $3.0^{+\infty}_{1.5}$ km s^{-1}. The other sight lines are assumed to be optically thin in the O I λ1356 transition.

[f] Abundance of interstellar gas-phase oxygen ($\pm 1\ \sigma$) per 10^6 H atoms in the observed sight lines. The uncertainties reflect the propagated N(H) and N(O I) errors.

◇ $N(H)$ is evaluated from 21cm emission and H_2 data

◇ $< n(H) >= N_H/d$ with d measured from parallax

◇ Results

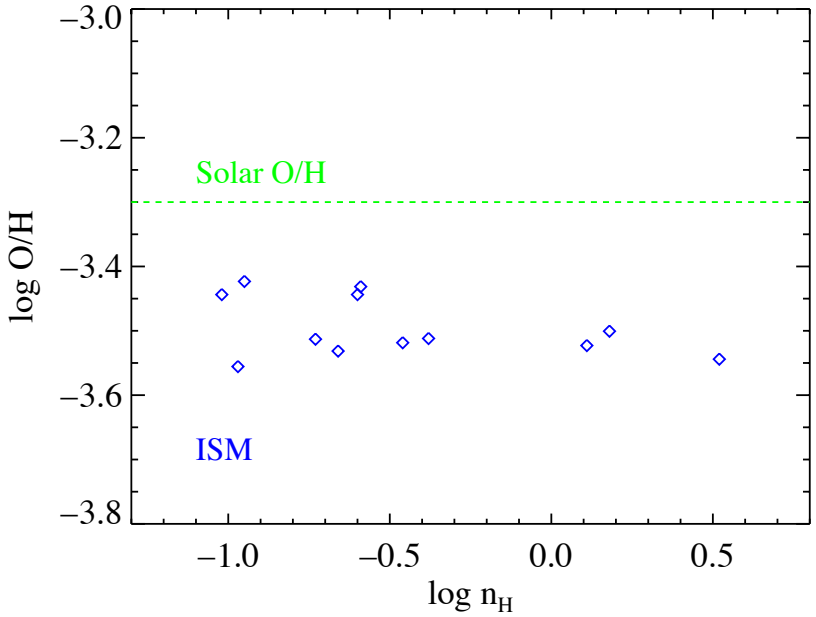

- Oxygen is uniformly distributed throughout the ISM
  - ◇ i.e. the ISM is well mixed
  - ◇ Presumably, the same is true for all elements

- ◇ Fuel for future star formation
- Modest offset between the ISM and the Sun
  - ◇ Error in the Solar determination? (it has dropped by 2× in the past decade)
  - ◇ Dust depletion? (Is some O locked up into dust grains?)

C. ISM Abundances: Other metals

- Dominant ionization state in an HI region
  - ◇ Consider the radiation field
    - ▲ The ISM has a very high opacity to radiation with $h\nu > 1$Ryd
    - ▲ But, it is optically thin to radiation with $h\nu < 1$Ryd
  - ◇ Ionization potential
    - ▲ IP(HI) = 13.6 eV
    - ▲ Majority of abundant elements have IP < 1Ryd for the first ionization state
    - ▲ Majority of abundant elements have IP > 1Ryd for the second ionization state
    - ▲ O^0, N^0, Ar^0 are obvious exceptions
    - ▲ Table

Complete Ionization Potentials for the First 10 Elements (eV)

Z	element	1st	2nd	3rd	4th	5th	6th	7th	8th	9th	10th
1	**H**	13.6									
2	**He**	24.6	54.4								
3	**Li**	5.4	75.6	122							
4	**Be**	9.3	18.2	154	218						
5	**B**	8.3	25.2	37.9	259	340					
6	**C**	11.3	24.4	47.9	64.5	392	490				
7	**N**	14.5	29.6	47.5	77.5	97.9	552	667			
8	**O**	13.6	35.1	54.9	77.4	114	138	739	871		
9	**F**	17.4	35.0	62.7	87.1	114	157	185	953	1103	
10	**Ne**	21.6	41.0	63.5	97.1	126	158	207	239	1196	1362

First 5 Ionization Potentials (eV) only, for other "A" group elements

Z	element	1st	2nd	3rd	4th	5th	Z	element	1st	2nd	3rd	4th	5th
11	**Na**	5.1	47.3	71.6	98.9	138	38	**Sr**	5.7	11.0	43.6	57	71.6
12	**Mg**	7.6	15.0	80.1	109	141	49	**In**	5.8	18.9	28.0	54	?
13	**Al**	6.0	18.8	28.4	120	154	50	**Sn**	7.3	14.6	30.5	40.7	72.3
14	**Si**	8.2	16.3	33.5	45.1	167	51	**Sb**	8.6	16.5	25.3	44.2	56
15	**P**	10.5	19.7	30.2	51.4	65.0	52	**Te**	9.0	18.6	28.0	37.4	58.8
16	**S**	10.4	23.3	34.8	47.3	72.7	53	**I**	10.5	19.1	33	?	?
17	**Cl**	13.0	23.8	39.6	53.5	67.8	54	**Xe**	12.1	21.2	32.1	?	?
18	**Ar**	15.8	27.6	40.7	59.8	75.0	55	**Cs**	3.9	25.1	?	?	?
19	**K**	4.3	31.6	45.7	60.9	82.7	56	**Ba**	5.2	10.0	?	?	?
20	**Ca**	6.1	11.9	50.9	67.1	84.4	81	**Tl**	6.1	20.4	29.8	?	?
31	**Ga**	6.0	20.5	30.7	64	?	82	**Pb**	7.4	15.0	31.9	42.3	68.8
32	**Ge**	7.9	15.9	34.2	45.7	93.5	83	**Bi**	7.3	16.7	25.6	45.3	56.0
33	**As**	9.8	18.6	28.4	50.1	62.6	84	**Po**	8.4	?	?	?	?
34	**Se**	9.8	21.2	30.8	42.9	68.3	85	**At**	9.5	?	?	?	?
35	**Br**	11.8	21.8	36	47.3	59.7	86	**Rn**	10.7	?	?	?	?
36	**Kr**	14.0	24.4	37.0	52.5	64.7	87	**Fr**	4	?	?	?	?
37	**Rb**	4.2	27.3	40	52.6	71.0	88	**Ra**	5.3	10.1	?	?	?

  - ◇ Low-ion: Dominant species of an element in an HI region
    - ▲ e.g. Fe^+, C^+, H^0, O^0
    - ▲ High-ions: Si^{+3}, C^{+3}
- Observations
  - ◇ Majority of resonance lines have $\lambda < 3000$Å

◇ UV spectroscopy is required ⇒ Space observatory

◇ HST: FOS, GHRS, STIS (COS?)

- Example: μCol (Howk et al. 1999)

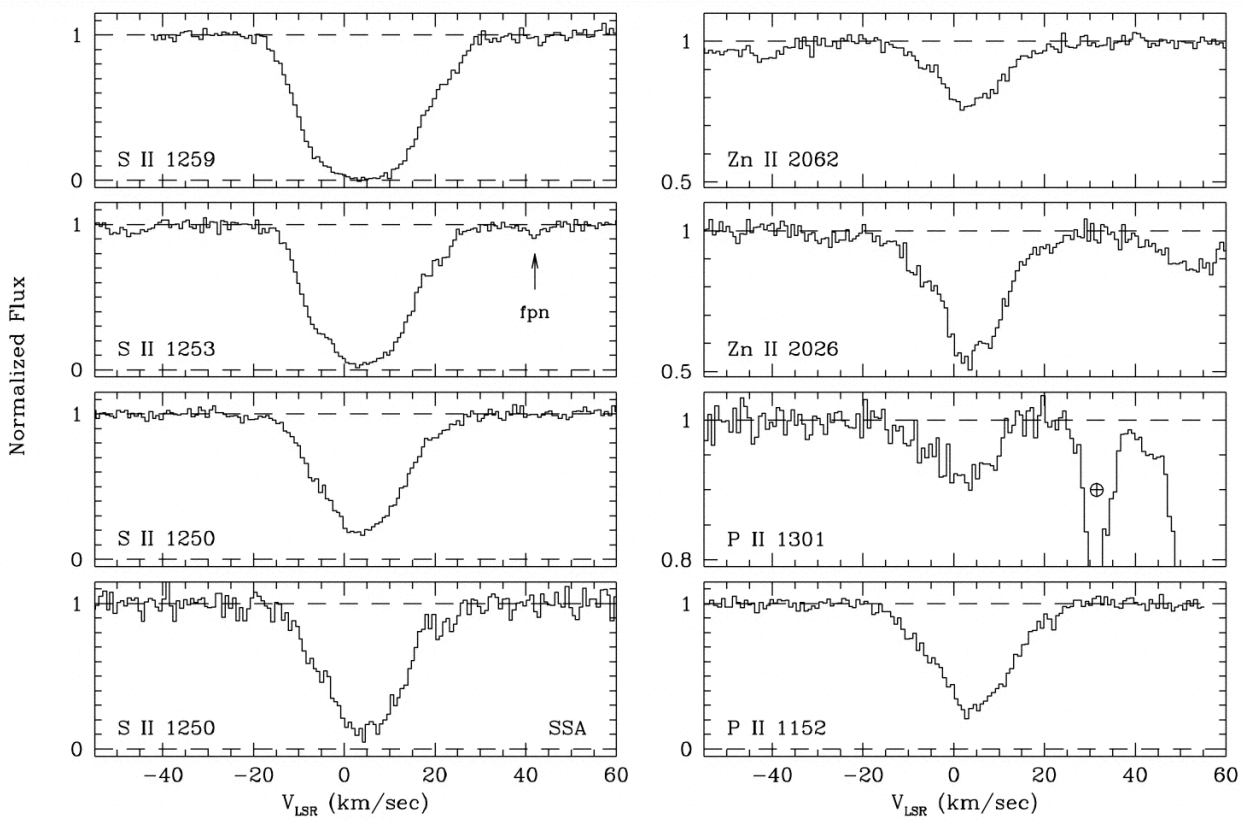

◇ Absorption lines are significantly offset from the stellar velocity → ISM

◇ Analysis

▲ Apparent optical depth method (Savage & Sembach 1991)

▲ Convert each pixel i into an apparent column density

$$N_a^i(v) = \frac{m_e c}{\pi e^2} \frac{\tau_a^i(v)}{f\lambda} \tag{7}$$

▲ Here, $\tau_a^i = \ln[I_i(v)/I_i^*(v)]$

▲ The column density is then

$$N_{TOT} = \int N_a^i(v) dv = \sum_i N_a^i \, (\Delta v)_i \tag{8}$$

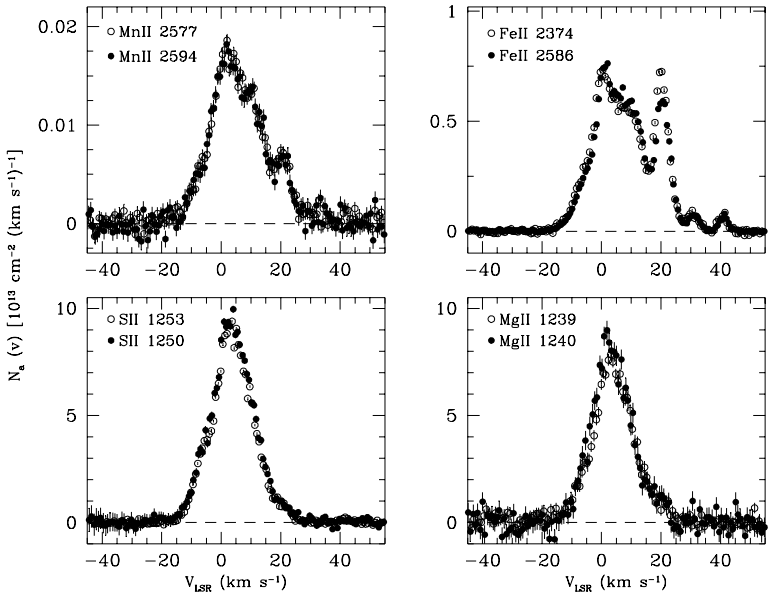

FIG. 9.—Representative plots of the $N_a(v)$ profiles for the ions Mn II, Fe II, S II, and Mg II. For most of the absorbing components, these profiles exhibit little in the way of unresolved saturated structure. The $N_a(v)$ profiles of Fe II are discrepant near $v_{LSR} \approx +20$ km s^{-1} (component 2), suggesting the presence of unresolved saturation in these transitions.

▲ Line profile fitting

◇ Column densities

▲ Table

TABLE 7
ADOPTED COLUMN DENSITIES

SPECIES	log N_X[a] cm^{-2}	log N_X (cm^{-2})[b] Comp 1 (3 km s^{-1})	Comp 2 (20 km s^{-1})	Comp 3 (31 km s^{-1})	Comp 4 (41 km s^{-1})
H I	19.86 ± 0.015[c]	...	...	...	...
C I.....	12.96 ± 0.03	12.87 ± 0.03	12.21 ± 0.09	...	...
C I*	$12.50^{+0.10}_{-0.12}$	$12.50^{+0.10}_{-0.12}$	...	...	...
C I**	<12.16	<12.16	...	...	...
C II	...	...	...	...	13.75 ± 0.05
C II*	...	...	13.23 ± 0.03	...	12.36 ± 0.05
N I	...	...	14.25 ± 0.08	...	13.17 ± 0.02
O I	<17.0[d]	...	...	13.58 ± 0.03	13.83 ± 0.02
Mg I.....	12.61 ± 0.02	12.55 ± 0.02	11.72 ± 0.02	10.28 ± 0.11	10.52 ± 0.04
Mg II	15.14 ± 0.02	15.08 ± 0.02[e]	13.95 ± 0.12	12.50 ± 0.02	12.82 ± 0.02
Al II	...	...	12.64 ± 0.05	11.47 ± 0.05	11.27 ± 0.06
Al III	12.01 ± 0.05	12.01 ± 0.05	...	...	...
Si II.....	15.14 ± 0.02	15.10 ± 0.02[f]	13.98 ± 0.05	12.78 ± 0.02	12.85 ± 0.02
Si II*	$11.47^{+0.12}_{-0.17}$	$11.47^{+0.12}_{-0.17}$	...	...	...
Si III	...	...	12.65 ± 0.08	11.83 ± 0.10	$10.84^{+0.16}_{-0.21}$
P II	13.48 ± 0.02	13.45 ± 0.02	11.98 ± 0.13	...	...
S II	15.21 ± 0.02	15.19 ± 0.02[g]	13.82 ± 0.02	<12.85	<12.85
S III.....	13.82 ± 0.02	13.82 ± 0.02	<12.59	<12.53	...
Ca II[h].....	12.35 ± 0.06	12.19 ± 0.08	11.85 ± 0.08	...	≤ 11.0
Ti II[i].....	11.84 ± 0.08	11.78 ± 0.09	10.95 ± 0.09	...	...
Cr II	12.62 ± 0.03	12.47 ± 0.04	12.03 ± 0.05	...	...
Mn II.....	12.55 ± 0.02	12.48 ± 0.02	11.61 ± 0.05	10.82 ± 0.09	10.55 ± 0.14
Fe II[j]	14.31 ± 0.01[k]	14.13 ± 0.02[k]	13.78 ± 0.02	12.63 ± 0.02	12.61 ± 0.02
Fe III	$13.37^{+0.09}_{-0.11}$	$13.37^{+0.09}_{-0.11}$	...	...	...
Ni II.....	12.98 ± 0.06[k]	12.86 ± 0.08[k]	12.35 ± 0.04	...	...
Cu II	<11.5	...	...	...	
Zn II.....	12.57 ± 0.08[k]	12.55 ± 0.08[k]	11.16 ± 0.08	...	...

[a] Total sightline column densities derived from integrations of $N_a(v)$ profiles, unless otherwise noted.
[b] Adopted column densities for the components considered here with $\pm 1\ \sigma$ errors, given in atoms cm^{-2}. Column densities for components 2–5 are derived from our component fitting analysis. Values for component 1 were derived through integrations of $N_a(v)$ profiles, unless otherwise noted.
[c] Derived using the continuum reconstruction method (see Appendix A).
[d] A 2 σ upper limit derived from the 1355.6 Å line.
[e] Based on the Mg II 1239, 1240 Å lines.
[f] Based on the Si II 1808 Å line.
[g] Based on the S II 1250 Å line.
[h] The Ca II data given here are from the profile-fitting results of Shull, York, & Witt 1977(see their Table 1).
[i] The Ti II data given here are from the profile-fitting results of Welsh et al. 1997 (see their Table 3). They have estimated the errors in the column density values to be ~10%–20%. The errors we have adopted in this table are slightly higher than this estimate.
[j] We have excluded the Fe II 2344 Å line and those lines with $\lambda < 1200$ Å in deriving this value because of possible oscillator strength uncertainties.
[k] The adopted column density given is derived from our component fitting measurements (see text).

◇ Relative abundances

▲ Define: [X/H] = log N(X)/N(H) - ($\epsilon_X - 12$)

▲ Tab

TABLE 9
NORMALIZED GAS-PHASE ABUNDANCES

ELEMENT X	log (X/H)[a] +12.00	[X/H][b]	[X/S][c] Comp 1 (3 km s^{-1})	[X/S][c] Comp 2 (20 km s^{-1})	[X/Si][d] Comp 3 (31 km s^{-1})	[X/Si][d] Comp 4 (41 km s^{-1})
C	8.55	...	...	...	...	-0.10 ± 0.06
N	7.97	...	...	...	...	-0.10 ± 0.03
O	8.87	...	...	...	-0.52 ± 0.04	-0.34 ± 0.03
Mg	7.58	-0.30 ± 0.02	-0.42 ± 0.03	-0.18 ± 0.12	-0.31 ± 0.03	-0.06 ± 0.03
Al	6.48	...	...	-0.39 ± 0.05	-0.24 ± 0.05	-0.51 ± 0.06
Si	7.55	-0.26 ± 0.02	-0.37 ± 0.03	-0.12 ± 0.06	...	...
P	5.57	$+0.05 \pm 0.02$	-0.04 ± 0.03	-0.14 ± 0.13	...	...
S	7.27	$+0.08 \pm 0.02$	...	...	...	...
Ti	4.93	-0.95 ± 0.09	-1.07 ± 0.05	-0.53 ± 0.09	...	...
Cr	5.68	-0.92 ± 0.03	-1.13 ± 0.04	-0.20 ± 0.05	...	...
Mn	5.53	-0.84 ± 0.02	-0.97 ± 0.03	-0.47 ± 0.05	$+0.06 \pm 0.09$	-0.28 ± 0.14
Fe	7.51	-1.06 ± 0.02	-1.30 ± 0.03	-0.28 ± 0.02	-0.11 ± 0.03	-0.20 ± 0.03
Ni	6.25	-1.13 ± 0.06	-1.31 ± 0.08	-0.45 ± 0.04	...	...
Zn	4.65	$+0.06 \pm 0.08$	-0.02 ± 0.08	-0.04 ± 0.08	...	...

[a] The logarithmic "solar" abundances of the elements, log (X/H)$_\odot$, are used in deriving the normalized gas phase abundances. We have adopted the solar system meteoritic abundances from Anders & Grevesse 1989 except for C, N and O, which are photospheric values from Grevesse & Noels 1993.

[b] We present the sightline integrated values of [X/H] in this column. Thus [X/H] $\equiv$ log $\{N_X/N_H\} -$ log $\{X/H\}_\odot$. Here we have used the value of log $N_{HI} = 19.86 \pm 0.015$ (1 σ systematic) derived in Appendix A as N_H. This treatment has neglected contributions from H^+. However, our photoionization modeling (see § 4) implies the corrections are relatively small (≈ -0.04 to -0.05 dex to the listed values).

[c] For the components 1 and 2 we have referenced the gas phase abundances to solar by comparing the column densities to that of sulfur. Thus [X/S] $\equiv$ log $\{N_X/N_S\} -$ log $\{X/S\}_\odot$.

[d] For components 3 and 4 we have referenced the gas phase abundances to solar by comparing the column densities to that of silicon. Thus [X/Si] $\equiv$ log $\{N_X/N_{Si}\} -$ log $\{X/Si\}_\odot$.

▲ Fig

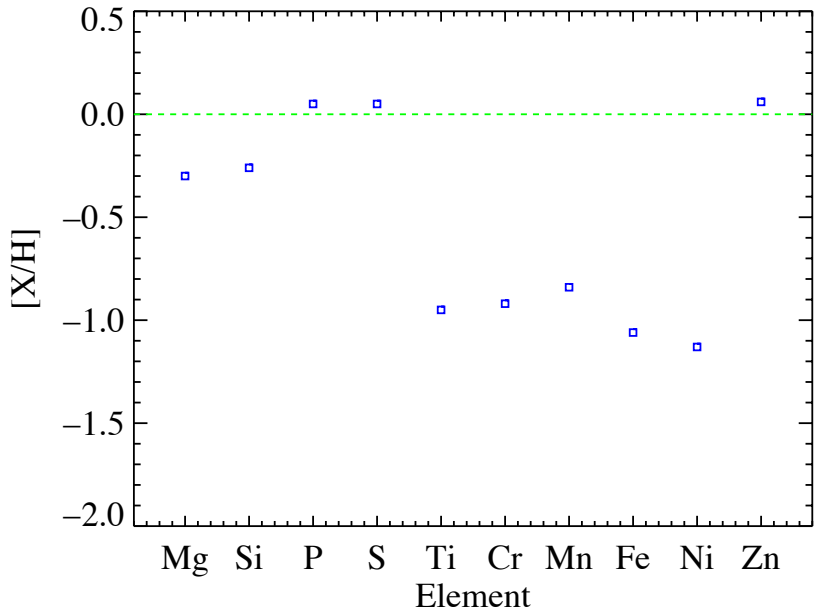

▲ S/H, Zn/H, P/H have roughly Solar values

▲ Why are Fe, Ni, Si, and Mn sub-solar?

▲ Does the ISM have a different nucleosynthetic pattern than the Sun?

D. Dust Depletion

- In the Galactic ISM, the majority of Fe, Si, Ni, Cr, and Ti are 'locked up' inside dust grains
  - ◇ Key point: We observe gas-phase abundances

◇ Consider Fe, which is highly refractory

$$N(\mathrm{Fe}) = N(\mathrm{Fe})_{gas} + N(\mathrm{Fe})_{dust} \tag{9}$$

▲ For $N(\mathrm{Fe})_dust > 0$, we have $[\mathrm{Fe/H}]_{gas} < 0$ in a solar metallicty gas

▲ Consider a cloud with $[\mathrm{Fe/H}]_{gas} = -1$

$$f_{gas} = \frac{M_{gas}}{M_{tot}} = 10^{[\mathrm{Fe/H}]_g} = 0.1 \tag{10}$$

- How do we know it is dust?
  - ◇ Redenning is observed
  - ◇ Extinction is inferred
- Condensation Temperature
  - ◇ G. Field: Observed winds for Red Giants
    - ▲ Observed Silicate absorption features
    - ▲ Concluded → Material contains dust grains
    - ▲ Grain forms as winds push gas off the Red Giant
    - ▲ This is the dominant mechanism for forming dust cores
  - ◇ T_C: Temperature at which 50% of the gas condenses into the solid phase
  - ◇ Expect smaller f_{gas} for higher T_C because it will have had a longer time to form dust
  - ◇ Plot [X/H] vs. T_C

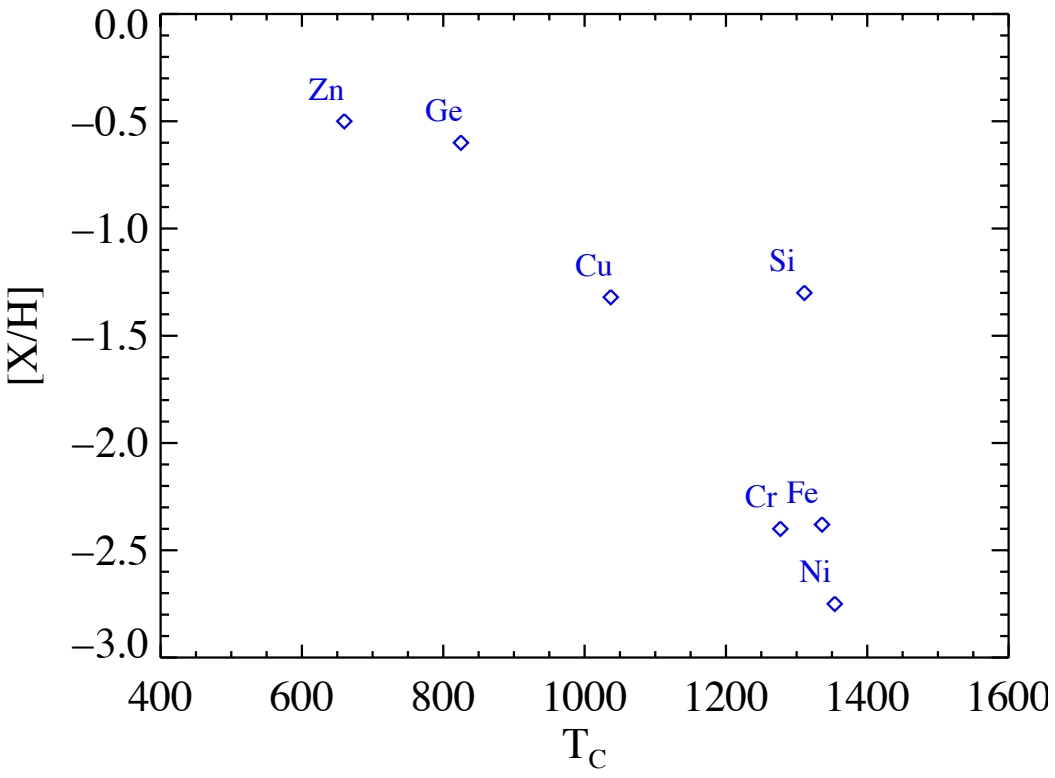

◇ Strong evidence that the observed gas-phase pattern of the ISM is due to dust, not nucleosynthesis

- Depletion/density relation
  - ◇ Jenkins (1986, 2003): Noted a correlation between n_H and depletion
  - ◇ Measure n_H
    - ▲ Observe 21cm emission
    - ▲ Determine the distance to the star
    - ▲ $< n_H >= N_{\rm HI}/d$ (ignoring H_2)
  - ◇ Examine the correlations

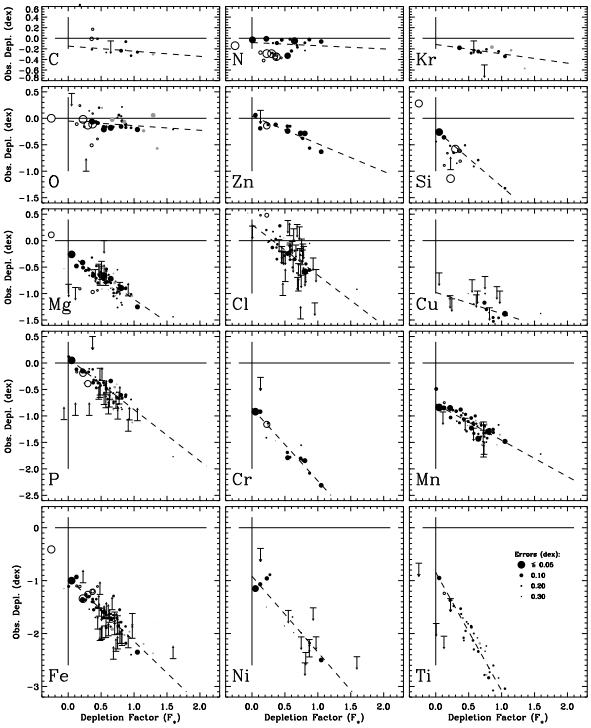

Figure 1: Observed element depletions as a function of the generalized line-of-sight depletion multiplier F_* defined in §1. In each case, the dashed line represents the best linear fit to Eq. 1 which ultimately defined the constants A_X (slopes) and $A_{0,X}$ (intercepts) listed by Jenkins (2003). Cases excluded in the best-fit

  - ◇ $F_* \propto n_H$, the volume density
  - ◇ Correlation indicates the environement (volume density) also influences grain formation
    - ▲ Dense clouds $\Rightarrow$ More two body interactions
    - ▲ Less dense clouds $\Rightarrow$ More susceptible to SN shocks which destroys grains
    - ▲ Environment affects the dust 'mantle' as append to the core

E. Interstellar Dust: Observations

- First evidence for dust:
  Robert Trumpler (1930), Lick Obs. Bull. 14, 154
  - ◇ Trumpler examined open clusters in the Galactic plane

◇ Chose a subset with similar richness and assumed they had similar physical origin

◇ Observed

▲ Apparent magnitude (m) of B and A stars

▲ Angular size (θ) of the cluster

◇ Determined

▲ Distance by adopting the absolute magnitude M for these stars according to their spectral type

$$5 \log d'_{pc} = m - M + 5 \tag{11}$$

▲ Physical size

$$\delta' = \theta d' \tag{12}$$

◇ Plotted the two quantities

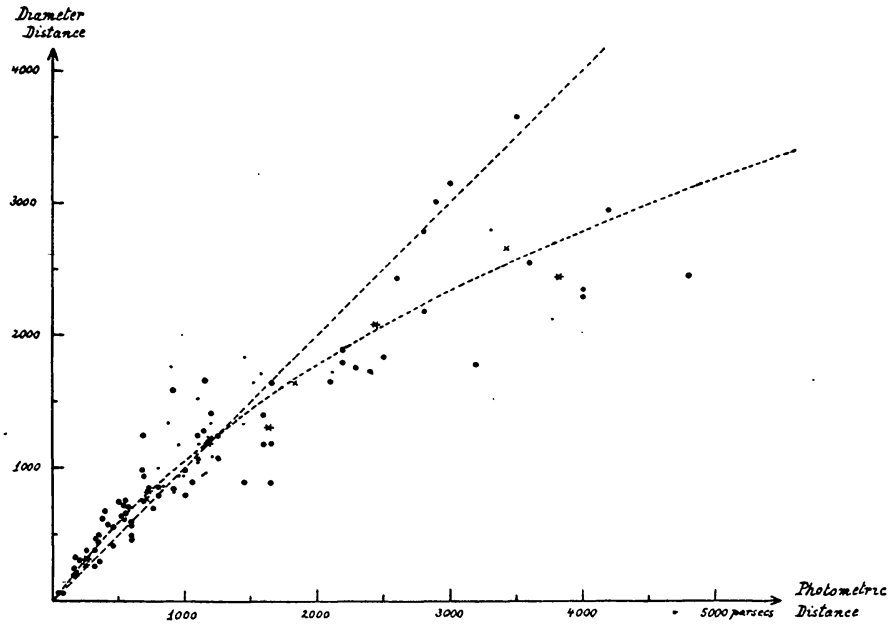

FIG. 1.—Comparison of the distances of 100 open star clusters determined from apparent magnitudes and spectral types (abscissae) with those determined from angular diameters (ordinates). The large dots refer to clusters with well-determined photometric distances, the small dots to clusters with less certain data (half weight). The asterisks and crosses represent group means. If no general space absorption were present, the clusters should fall along the dotted straight line; the dotted curve gives the relation between the two distance measures for a general absorption of $0^m.7$ per 1000 parsecs.

▲ Observed a rising δ' with increasing d'

▲ But the assumptions was that all of these clusters had the same δ' !

◇ Introduced dust

$$5 \log d = m + M + 5 - ad \tag{13}$$

▲ a is an extinction (photographic magnitudes/kpc)

▲ Trumpler adjusted a until δ' was constant

▲ Determined

$$a = 0.8\text{photomag/kpc} \tag{14}$$

- Other evidence for dust
  (a) dark clouds with a relative absence of stars
  (b) reflection nebula (Rayleigh scattering)
  (c) reddeining of starlight and extinction
  (d) polarization of starlight by aligned, non-spherical dust grains
  (e) IR continuum emission
  (f) diffuse galactic light – scattered from stars
  (g) depletion of Fe, Si, Ca, etc. from the gas phase
  (h) existance of large masses of H_2 – formed on grains
  (i) X-ray halos around point sources behind dust

F. Dust Absorption and Scattering

- General
  ◇ Dust scatters and absorbs light in the ISM
  ◇ Remits light at much longer wavelengths (IR)
- Extinction
  ◇ Ignore remission by dust
  ◇ Radiative transfer

$$I_\nu = I_\nu^* \mathrm{e}^{-\tau_\nu} \tag{15}$$

  ◇ Define extinction (in magnitudes)

$$A_\lambda = 1.086\tau_\lambda = 1.086 N_d Q_e(\lambda)\sigma_d \tag{16}$$

  ▲ N_d = Column density of dust
  ▲ σ_d = Mean physical grain cross-section
  ▲ Q_e = Efficiency coefficient for extinction

  ◇ In this case

$$A_\lambda = -2.5 \log \frac{F_\nu}{F_\nu(0)} \tag{17}$$

$$m_\lambda - M_\lambda = -5 + 5 \log d_{pc} + A_\lambda \tag{18}$$

- Extinction efficiency factor

$$Q_e \equiv \frac{s_\nu}{\sigma_d} \tag{19}$$

  ◇ s_ν = The optical cross-section (Thielens uses C_{ext})
  ◇ Q_e is the sum of absorption and scattering

$$Q_e(\lambda) = Q_a(\lambda) + Q_s(\lambda) \tag{20}$$

◇ Define albedo

$$\tilde{w}(\lambda) = \frac{Q_s(\lambda)}{Q_e(\lambda)} \tag{21}$$

- Mie theory
  - ◇ See Bohrem & Huffman (1983)
  - ◇ Index of refraction: m

$$m = n - ik \tag{22}$$

▲ Or, equivalently the dielectric constant

$$\epsilon = \epsilon_1 + i\epsilon_2 \tag{23}$$
$$\epsilon_1 = n^2 + k^2 \tag{24}$$
$$\epsilon_2 = 2nk \tag{25}$$
$$m = \sqrt{\epsilon} \tag{26}$$

◇ Consider a spherical dust grain with radius a and an incident wave with wavelength λ

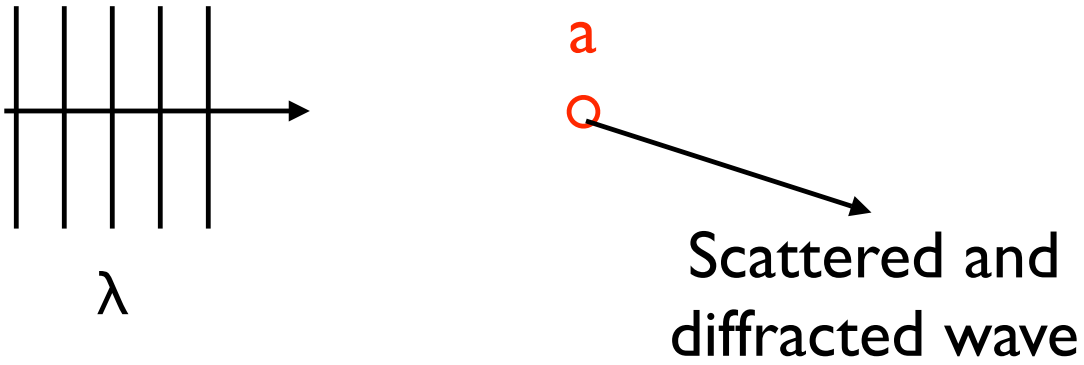

▲ Wave will be scattered and diffracted

▲ One needs to consider the propagation of the EM wave inside the dust grain (a medium)

◇ Plane wave travelling in the $\hat{z}$ direction

$$E = E_0 \exp\left[\, i\kappa z - i\omega t \,\right] \tag{27}$$

▲ In free space (vacuum)

$$\kappa = \frac{\omega}{c} = \frac{2\pi}{\lambda} \tag{28}$$

▲ In a medium with index of refraction m, $\kappa = \omega m/c$, and

$$E = E_0 \exp\left[-\frac{\omega}{c} z\right] \exp\left[-i\omega\left(t - \frac{nz}{c}\right)\right] \tag{29}$$

- ○ The real part (n) introduces a phaes shift, i.e. a phase velocity $v = c/n$
- ○ The imaginary part (k) introduces a damping

- We conclude that any system that produces absorption will also produce dispersion

◇ Mie theory involves expanding Q in a series expansion in x

$$x \equiv \frac{2\pi a}{\lambda} \tag{30}$$

◇ Rayleigh limit

▲ Small x, i.e. $a \gg \lambda$

▲ We need only retain the leading terms in x

$$Q_a = \frac{\sigma_{abs}(x)}{\pi a^2} = -4x \,\mathrm{Im}\left(\frac{m^2-1}{m^2+2}\right) \tag{31}$$

$$Q_s = \frac{\sigma_{scatt}(x)}{\pi a^2} = \frac{8}{3}x^4 \,\mathrm{Real}\left[\frac{m^2-1}{m^2+2}\right] \tag{32}$$

$$Q_e = Q_a + Q_s \tag{33}$$

▲ Wavelength dependence

- $Q_a \propto \lambda^{-1}$ which is as observed
- $Q_s \propto \lambda^{-4}$, i.e. the Rayleigh scattering expression

• Q evolution with x (Spitzer, Fig 7.1)

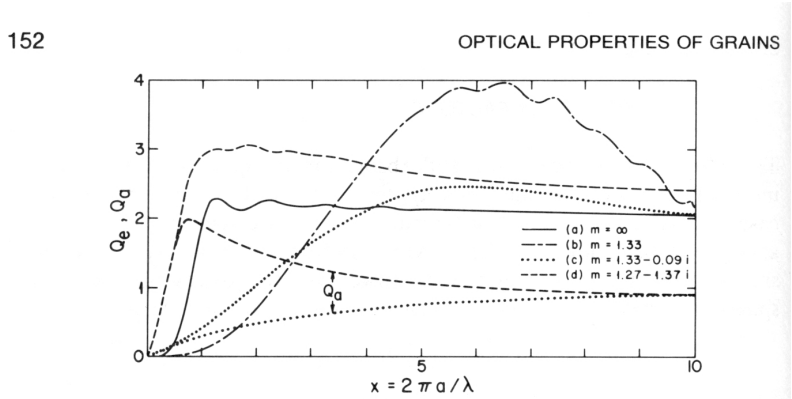

Figure 7.1 Extinction and absorption cross section for spheres. For each value of m, the index of refraction, the upper curves show Q_e, the ratio of extinction and geometrical cross sections, for spheres; x is the ratio of the circumference, $2\pi a$, to the wavelength, λ, of the incident radiation. For cases (c) and (d), with complex values of m, lower curves show Q_a, the corresponding ratio of absorption cross section to πa^2. These theoretical curves [1] are based on exact computations for cases (a), (b), and (d), but for case (c), on an approximate theory, valid for small $m-1$.

◇ Note the action at small x

▲ $Q_a \propto x$

▲ $Q_s \propto x^4$

▲ $Q_a \gg Q_s$

◇ Note: $Q_e \to 2$ as $x \to \infty$

- ▲ The particle absorbs an area πa^2
- ▲ The particle diffracts an equal amount!

- Integral over Q_e: Kramers-Kronig

$$\int_0^\infty Q_e d\lambda = 4\pi a^2 \left(\frac{\epsilon_0 - 1}{\epsilon_0 + 2} \right) \equiv 4\pi a^2 F_K \tag{34}$$

  - ◇ ϵ_0 is the dielectric constant of the grain in the low frequency limit $\epsilon_0 = m^2$
  - ◇ F_K is as defined

- Grains also absorb momentum
  - ◇ For an EM wave with flux F_0, the momentum imparted is

$$\frac{F_0}{c}\pi a^2 Q_a + \frac{F_0}{c}\pi a^2 Q_s \left(1 - < \cos\theta > \right) \tag{35}$$

  - ◇ Define

$$Q_{pr} = Q_a + Q_s \left(1 - < \cos\theta > \right) \tag{36}$$

$$= Q_e - Q_s < \cos\theta > \tag{37}$$

    - ▲ One often introduces a "phase factor" for scattering

$$g(\theta) \equiv < \cos\theta > \tag{38}$$

    - ▲ Limits
      - ○ $< \cos\theta >= 0$ is isotropic
      - ○ $< \cos\theta >= -1$ is back scattering
      - ○ $< \cos\theta >= +1$ is forward scattering
  - ◇ Force on the grains

$$f = \frac{F_0}{c}\pi a^2 Q_{pr} \tag{39}$$

G. Grain Temperature

- Heating processes
  - ◇ Absorption of starlight (dominant)

$$H_{rad} = \int Q_a(\lambda) \frac{1}{4} u_\lambda c 4\pi a^2 d\lambda \tag{40}$$

  - ◇ Collisions with gas particles
  - ◇ Exothermic chemical reactions on the grain surface
- Cooling
  - ◇ Emission of IR radiation

◇ In thermal equilibrium

$$\kappa_\lambda B_\lambda = j_\lambda \tag{41}$$

$$n_d Q_a \pi a^2 B_\lambda = n_d \frac{\varepsilon_\lambda}{4\pi} \tag{42}$$

$$\varepsilon_\lambda = Q_a \pi a^2 \cdot \pi B_\lambda \tag{43}$$

◇ Radiative losses (per particle)

$$L_{rad} = \int Q_a(\lambda) \pi B_\lambda(T_d) 4\pi a^2 d\lambda \tag{44}$$

- Estimate the temperature

$$\pi a^2 c \int Q_a(\lambda) u_\lambda d\lambda = 4\pi a^2 \int Q_a(\lambda) \pi B_\lambda(T_d) d\lambda \tag{45}$$

◇ Let u_λ = optical and near-UV energy density ($u \approx 7 \times 10^{-13}$ erg/cm^{-3})

◇ Assume (first), that $Q_a(\lambda) \approx 1$

◇ Blackbody

$$B = \int B_\lambda d\lambda = \frac{\sigma T_d^4}{\pi} \tag{46}$$

◇ Reduce..

$$cu = \pi B(T_d) \tag{47}$$

$$T_d = \left(\frac{cu}{4\sigma} \right)^{1/4} = 3.1\,\mathrm{K} \tag{48}$$

◇ But, the IR excess from the Galactic plane implies $T_d = 20$K !!
What went wrong?

- Recall that Mie theory indicates $Q_a \propto \lambda^{-1}$

◇ Therefore $Q_a(\mathrm{UV}) > Q_a(\mathrm{IR})$

◇ Approximate the ISM diffuse starlight as a dilute blackbody with $T_R = 10^4$K

◇ Express

$$u_\nu = \tilde{u} \frac{\nu^3}{\mathrm{e}^{h\nu/kT_R} - 1} \tag{49}$$

◇ Our equilibrium equation becomes

$$\tilde{u} \int_0^\infty \frac{\nu^3 Q_a(\nu)}{\mathrm{e}^{h\nu/kT_R} - 1} d\nu = \int_0^\infty \frac{\nu^3 Q_a(\nu)}{\mathrm{e}^{h\nu/kT_d} - 1} d\nu \tag{50}$$

▲ Let $x \equiv h\nu/kT$

▲ Evaulate

$$\tilde{u} T_R^5 I_4 = T_d^5 I_4 \tag{51}$$

$$I_4 = \int_0^\infty \frac{x dx}{\mathrm{e}^x - 1} \tag{52}$$

◇ Therefore

$$T_d = \tilde{u}^{1/5} T_R \tag{53}$$

▲ $\tilde{u}$ is related to the geometric dilution of starlight

▲ $\tilde{u} \approx 10^{-14}$

▲ Therefore, $T_d \approx 16$K

- Other expressions

◇ One can write Equation 53 as

$$T_d = \left(\frac{hc}{k} \right) \left[\frac{4\pi J}{384\pi^2 a h c^2 \zeta(5)} \right]^{1/5} \tag{54}$$

▲ This gives

$$T_d = 9 \left(\frac{1\mu\,\mathrm{m}}{a} \right)^{0.2} \mathrm{K} \tag{55}$$

▲ Grains are also somewhat hotter than above because they are less efficient at emitting at UV and optical wavelengths

▲ There are also dependencies on composition

$$T_{\mathrm{Silicon}} = 13.6 \left(\frac{1\mu\,\mathrm{m}}{a} \right)^{0.06} \mathrm{K} \tag{56}$$

$$T_{\mathrm{Graphite}} = 15.2 \left(\frac{1\mu\,\mathrm{m}}{a} \right)^{0.06} \mathrm{K} \tag{57}$$

$$\tag{58}$$

- **Dust Density**

◇ Recall our definition for extinction

$$A_V = 1.086 \tau_V = 1.086\, n_d\, \ell\, Q_e(V) \pi a_d^2 \tag{59}$$

◇ Adopt $A_V = 2, \ell = 1, Q_e = 2$

$$n_d \approx 1.0 \times 10^{-12} \left(\frac{a_d}{10^{-5}\mathrm{cm}} \right)^2 \mathrm{cm}^{-3} \tag{60}$$

◇ Mass density

$$m_d n_d = \frac{4}{3} \pi a_d^3 \rho_d n_d = 4.3 \times 10^{-27} \rho_d \left(\frac{a_d}{10^{-5}\mathrm{cm}} \right) \mathrm{g/cm}^3 \tag{61}$$

▲ For ice grains

$$\rho_D \sim 1 \mathrm{\ g/cm}^3 \tag{62}$$

$$a_D \sim 0.3\mu \tag{63}$$

▲ Therefore

$$m_d n_d = 10^{-26}\ \mathrm{g/cm^3} \tag{64}$$

◇ Dust to gas ratio

▲ Take $n_H \sim 1\,\mathrm{cm^{-3}}$

$$\frac{\rho_d}{\rho_g} = \frac{10^{-26}\mathrm{g/cm^3}}{(1\,\mathrm{cm^{-3}})2 \times 10^{-24}\mathrm{g}} \approx 10^{-2} \tag{65}$$

▲ Compare this against the value you get by assuming 100% of the Fe, Si, and Mg is in dust and also 2/3 of the C

H. Extinction Laws

- Differential extinction

◇ Observe two stars with identical spectral type

$$\Delta m(\lambda) \equiv m_2(\lambda) - m_1(\lambda) \tag{66}$$
$$= 5\log d_2 - 5\log d_1 + M_2 - M_1 + A_2(\lambda) - A_1(\lambda) \tag{67}$$

▲ OB stars are best as they vary less with T

▲ Also, they are very bright

◇ Observe the stars at two wavelengths

$$\Delta m(\lambda_a) - \Delta m(\lambda_b) = [\,A_2(\lambda_a) - A_1(\lambda_a)\,] - [\,A_2(\lambda_b) - A_1(\lambda_b)\,] \tag{68}$$
$$= \Delta\,(\,A(\lambda_a) - A(\lambda_b)\,) \tag{69}$$
$$\equiv E(\lambda_a - \lambda_b) \tag{70}$$

▲ $E(\lambda_a - \lambda_b)$ is referred to as the color excess

▲ Generally, one defines the color excess in the B and V bands

$$E_{B-V} = A(\lambda_B) - A_(\lambda_V) = A_B - A_V \tag{71}$$
$$\lambda_B \approx 4350\text{Å} \tag{72}$$
$$\lambda_V \approx 5550\text{Å} \tag{73}$$

- Extinction curves

◇ Define the selective extinction by normalizing relative to E_{B-V}

$$e(\lambda) = \frac{E_{\lambda-V}}{E_{B-V}} = \frac{A_\lambda - A_V}{A_B - A_V} \tag{74}$$

◇ Define the ratio of total to selective extinction

$$R_V \equiv \frac{A_V}{E_{B-V}} \tag{75}$$

▲ $R_V \approx 3.1 - 3.3$ in the Milky Way

- ▲ $R_V = 3.1$ is generally assumed but not well measured
- ▲ Larger R_V implies larger dust grains

◇ Milky Way extinction curve

- ▲ Empirically measured
- ▲ Fitted by Cardelli et al. (1989)
- ▲ Fig (assumes $R_V = 3.1$)

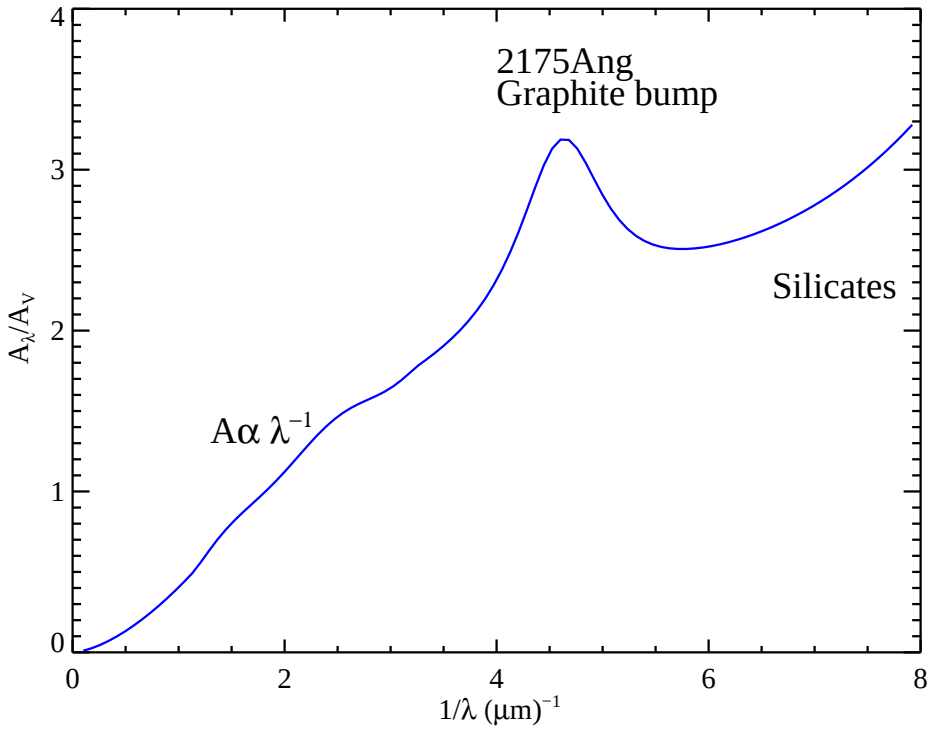

◇ Other empirical extinction curves

- ▲ Empirically measured for LMC, SMC
- ▲ Synthesis curve for starbursts (Calzetti)

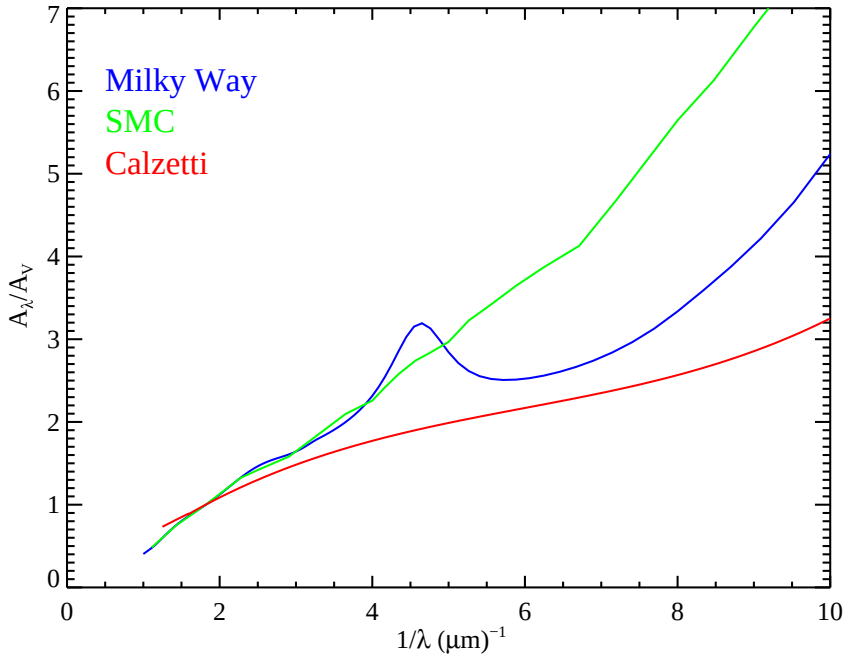

◇ Generic extinction law – Fitzpatrick & Massa (1990)

▲ Analyzed extinction throughout the Milky Way and found a single law was not applicable

▲ Introduced a fitting function to allow for variations

$$e(\lambda) = c_1 + c_2 x + c_3 D(x;\gamma,x_0) + c_4 F(x) \tag{76}$$

$$x \equiv \lambda^{-1} \tag{77}$$

$$D(x;\gamma,x_0) = \frac{x^2}{\left(x^2 - x_0^2\right)^2 + x^2\gamma^2} \tag{78}$$

$$F(x) = 0.5392(x-5.9)^2 + 0.05644(x-5.9)^3 \quad [x \geq 5.9\,\mu\mathrm{m}^{-1}] \tag{79}$$

○ c_2 gives a linear 'background' term

○ c_3 parameterizes the 2175Å bump

○ c_4 parameterizes the far-UV extinction

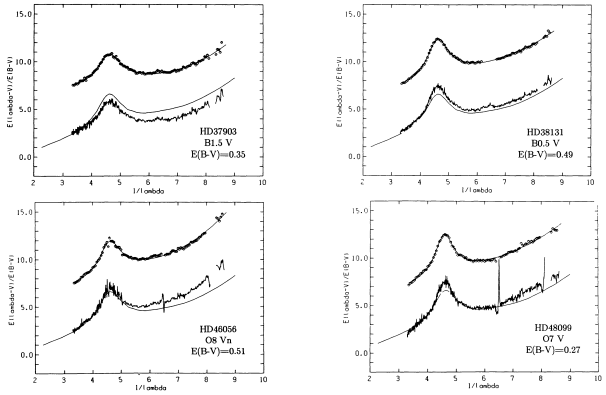

- Some useful relations (Milky Way)

$$A_V = 2\,\mathrm{mag/kpc} \;\; (R_V = 3.1) \tag{80}$$
$$E_{B-V} = 0.61\,\mathrm{mag/kpc} \tag{81}$$
$$N_H = 5.9 \times 10^{21}\, E_{B-V} \;=\; 2 \times 10^{21} A_V \;\; \mathrm{cm}^{-2} \tag{82}$$

I. Polycyclic Aromatic Hydrocarbons (PAHs)

- Not dust, but large molecules
  - ◇ Likely to dominate the observed 2175Å extinction bump
  - ◇ Dominate IR emission near 12μm
- Structure
  - ◇ Planar molecule consisting of C atoms in a honeycombed lattice
  - ◇ Fused six-membered 'rings' with H atoms at the edges
  - ◇ Fig 6.1 of Thielens

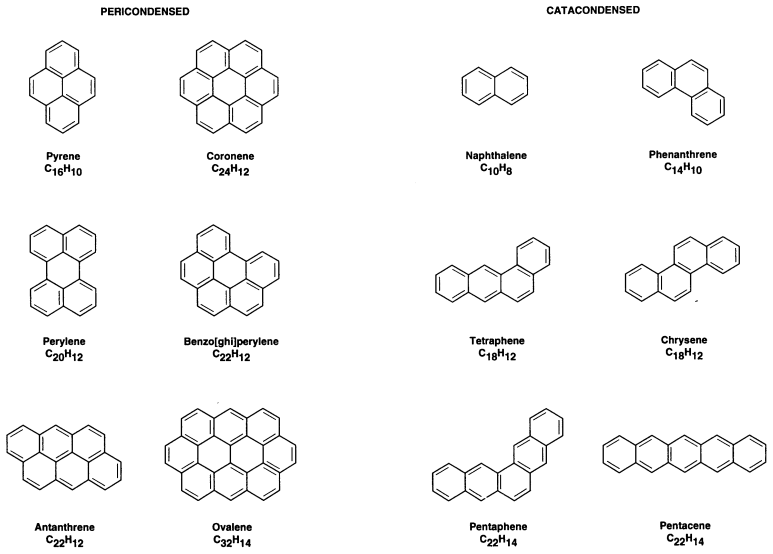

- Size and surface area
  - ◇ C-C bonds are ≈ 1.4Å long
  - ◇ A ring has an area of ≈ 5Å^2
  - ◇ For a PAH composed of N_C atoms:

$$\sigma_{\mathrm{PAH}} = 5 \times 10^{-16}\, N_{\mathrm{C}} \;\mathrm{cm}^{-2} \tag{83}$$

    - ▲ A PAH with 50 C atoms has $\sigma_{\mathrm{PAH}} \approx 200$Å^2 and size of 6Å
    - ▲ More typical are PAHs with 10^4 to 10^5 C atoms giving sizes of 30 to 60Å
    - ▲ Compare with dust which ranges from 50 to 3000Å
- IR emission

- ◇ Complex molecular physics
  - ▲ C-H, C-C stretching modes
  - ▲ C-H bending modes
  - ▲ etc.
- ◇ Also, complicated temperature distribution
- ◇ Bottom line, beware the challenges of estimating the IR emission for PAHs from astrophysical sources
- ◇ Peeters et al. 2002, A& A, 390, 1089

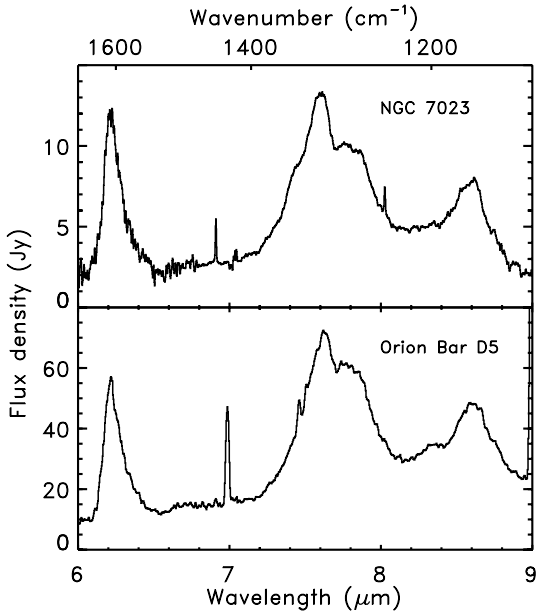

Fig. 3. Two examples to show the richness of the 6–9 μm region. We recognise the 6.2 and 8.6 μm features. The 7.7 μm feature breaks up in three components; two clear bands at 7.6 and 7.8 μm and a shoulder at 7.4 μm. Furthermore, weak features are present at 6.6 and 8.2 μm.

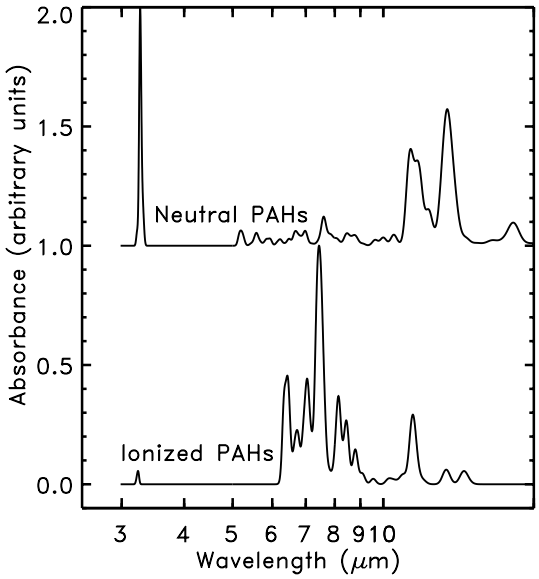

Fig. 21. The absorption spectrum of a mixture of neutral PAHs **a)** compared to the spectrum of the same PAHs in their positive state **b)**. This comparison shows that, for PAH spectra, ionisation has a much greater influence on relative intensities than on peak frequencies, with the features in the 6 to 10 μm region substantially enhanced with respect to the rest of the spectrum (Figure adapted from Allamandola et al. 1999).